J. Fluid Mech. (1966), *vol.* 26, *part* 1, *pp.* 199–221
Printed in Great Britain

A study of turbulence at a wall using an electrochemical wall shear-stress meter

By JAMES E. MITCHELL AND THOMAS J. HANRATTY

Department of Chemistry and Chemical Engineering,
University of Illinois, Urbana, Illinois

(Received 11 September 1965 and in revised form 4 April 1966)

A technique has been developed to measure the instantaneous shear stress at the boundary over which a liquid is flowing. It is being used to study turbulence in the immediate vicinity of a pipe wall. A reaction is conducted on an electrode mounted flush with a solid wall at high enough voltages to reduce the concentration of the reacting species to zero at the surface. Under these conditions, the rate of reaction is controlled by the rate of mass transfer. The electrode is analogous to a constant-temperature hot-wire anemometer in that the surface concentration is kept constant and the current flowing in the circuit is related to the surface shear stress. For fully developed turbulence the limiting velocity intensity, based on the local average velocity, is 0·32. Some of the velocity fluctuations are as large as the local average velocity and their distribution is nearly symmetric about the average. The ratio of the longitudinal to circumferential scale is about 30 : 1, because the circumferential scale is very small. There is some indication that close to a wall the velocity fluctuations in the circumferential direction are much smaller than the longitudinal fluctuations.

1. Introduction

Measurements of time-averaged velocities for turbulent flow over a solid boundary have shown a region close to the wall, known as the viscous sub-layer, in which the transfer of momentum by turbulent velocity fluctuations is negligible compared with transfer by molecular viscosity. Studies of temperature profiles and concentration profiles have indicated that the portion of the flow field in which turbulent transport of heat or mass is negligible (the diffusion sub-layer) depends on the relative magnitudes of the kinematic viscosity to the molecular diffusivities of heat or mass; that is, the Prandtl number or the Schmidt number. For large Prandtl number or large Schmidt number the diffusion sub-layer is much smaller than the viscous sub-layer and the unsteady flow in the viscous sub-layer must be taken into account in order to predict rates of heat and mass transfer.

Although the turbulent transfer of momentum may be neglected in the viscous sub-layer the magnitude of the velocity fluctuations is quite large compared with the local average velocity. It is of considerable importance to have detailed measurements of the fluctuating flow in the immediate vicinity of a wall. Such studies would not only yield a better understanding of turbulent transport but would also be helpful in determining the structure of turbulent shear flow. Yet

it is quite difficult to obtain this information, owing to the smallness of the viscous sub-layer.

Reiss & Hanratty (1962, 1963) have estimated the velocities in the region $y^+ < 0{\cdot}5$ using a diffusion-controlled electrode mounted flush with the wall. This technique has advantages over visual studies in that it yields quantitative information more easily. It has advantages over the hot-wire anemometer in that it introduces no disturbances and yields measurements of the velocity field much closer to the wall.

The electrochemical technique used by Reiss & Hanratty is analogous to the constant-temperature hot-wire anemometer in that the concentration of the diffusing species is constant at the electrode surface and the current is proportional to the rate of mass transfer to the electrode. These mass-transfer measurements are related to the velocity gradient at the wall in which the electrode is contained. The problems involved in defining this relation are similar to those encountered in relating hot-wire anemometer measurements to the fluctuating velocity field. One is concerned about non-uniform flow across the probe and about the response of the instrument to fluctuations in the velocity field. The electrode exhibits an effect similar to that associated with the heat capacity of the hot wire in that the concentration boundary layer over the electrode surface causes a response which is not in phase with the velocity fluctuations. Reiss & Hanratty used circular electrodes. This choice of geometry did not allow for the examination of the effect of electrode width and the effect of the time response independently. Furthermore, because of the large centre-to-centre distance between adjacent circles, the electrodes could not be used to measure the circumferential correlation coefficients accurately enough to correct for non-uniform flow. The work of Reiss & Hanratty has been extended in a recent study by Mitchell (1965), and the relation between mass-transfer measurements and the velocity field has been defined more accurately. By using electrodes with a rectangular shape the orientation, the length and the width of the probes could be selected independently. The freedom of orientation allows the use of electrodes placed at 45° to the flow for the measurement of circumferential velocity components and ones at 90° for the longitudinal components. The separation distances between probes were reduced to small enough values that correlation data in the circumferential direction could be taken and a reliable correction for non-uniform flow could be achieved. Variation of the width of several electrodes made it possible to verify this correction by a set of independent measurements. Mitchell obtained a solution for the time response of the concentration boundary layer by a direct numerical method. It has been found that the approximate solution used by Reiss & Hanratty over estimated the effect by a large amount. Measurements of the velocity intensities with several electrodes of different lengths made it possible to check this calculation.

This paper has been written to summarize results of the studies carried out in this laboratory by Mitchell and Reiss & Hanratty. It has two purposes. First, it shows how electrochemical techniques can be used to measure the time-averaged and the fluctuating wall shear stress. Secondly, it presents new measurements of the properties of turbulent shear flow in the immediate vicinity of a wall.

2. Application of electrochemical techniques to measure the wall shear stress

The test electrode is part of an electrochemical cell made up of an aqueous solution of potassium ferri- and ferrocyanide and nickel electrodes. This reaction has been used by Eisenberg, Tobias & Wilke (1954) for the measurement of average mass-transfer rates from rotating cylinders, and by Gordon & Tobias (1963) for the measurement of diffusion coefficients for the ferricyanide ion. The electrolyte is pumped through a flow loop where portions of the pipe wall serve as electrodes. The measuring electrodes are enclosed in the wall of a 1 in. I.D. 'Lucite' pipe. The test section is preceded by a straight length of pipe of 180 pipe diameters to ensure that the flow is fully developed. The anode is a U-bend made of nickel pipe located downstream of the test section. The electrolyte has a composition of 0·01 molar potassium ferricyanide, 0·01 molar potassium ferrocyanide, and 2 molar sodium hydroxide. The sodium hydroxide acts as a low-resistance vehicle for current flow throughout all of the cell except very near the electrodes. The following reactions occur at the surfaces of the electrodes:

$$\text{cathode (test electrode) } Fe(CN)_6^{3-} + e \rightleftarrows Fe(CN)_6^{4-};$$

$$\text{anode (reference electrode) } Fe(CN)_6^{4-} \rightleftarrows Fe(CN)_6^{3-} + e.$$

If these are the only reactions occurring in the system then the current flowing I is related to rate of reaction of ferricyanide per unit area of test electrode N:

$$N = (I/AF)(1-T), \tag{1}$$

where A is the area of the test electrode, F is Faraday's constant, and T is the transference number. Owing to the large concentration of sodium hydroxide relative to ferricyanide the transference number is approximately 0·001 and can be neglected. Since oxygen reacts cathodically at a voltage near that used in the experiments, the solution is purged of dissolved oxygen and the experiment is conducted under an atmosphere of nitrogen. Because of the corrosive nature of the electrolyte, precautions had to be taken in selecting the materials of construction for the flow loop.

A mass-transfer coefficient K can be defined as

$$K = N/(C_b - C_w), \tag{2}$$

where C_b is the bulk concentration of the ferricyanide ion and C_w is the concentration at the surface of the electrode. Since the area of the reference electrode is much larger than the area of the test electrode C_w is much smaller on the test electrode. The current increases with the voltage across the electrodes until at high enough voltages there is no further increase. Under these conditions C_w is essentially zero at the test electrode and the current flowing through the circuit is controlled by the rate of mass transfer to test electrode. The current will then vary directly as K, which depends on the velocity field in the vicinity of the test electrode. In the experiments reported in this paper the thickness of the concentration boundary layer was less than $y^+ = 0{\cdot}5$ and therefore the measured values of K reflect the properties of the velocity field for $y^+ < 0{\cdot}5$. The concentration

boundary layer is thin because the Schmidt number is very high (approximately 2300). Owing to the thinness of the region over which the velocity field is sampled, a mathematical model can be constructed which assumes the velocity normal to the surface is zero and the velocity in the plane of the surface equals the product of the wall velocity gradient and the distance from the wall. Consequently, the technique yields measurements of the steady and fluctuating shear stresses at the wall.

3. Electrode design

The test electrodes were constructed by inserting circular wires or nickel sheet through the wall and gluing them in place. The protruding metal was smoothed flush with the pipe wall by hand-sanding with progressively finer grades of emery

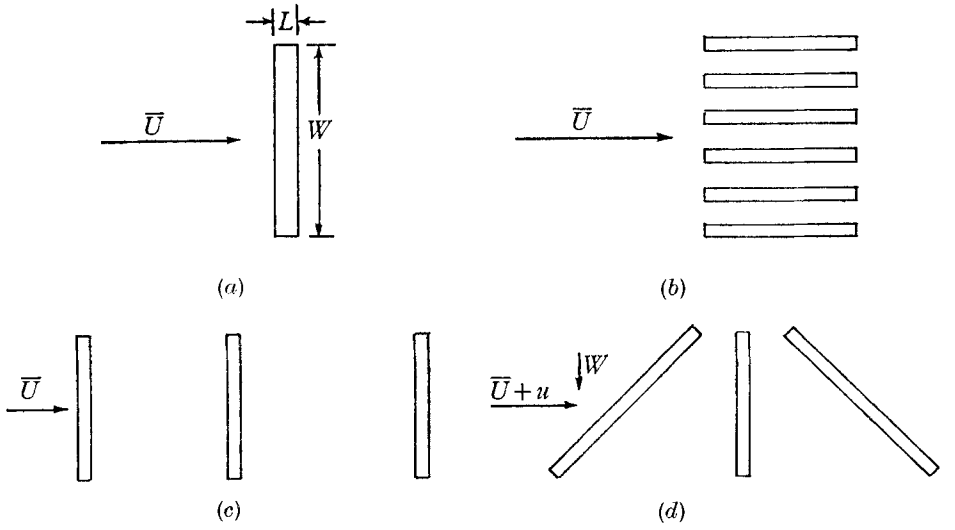

FIGURE 1. Electrode configuration for various measurements. (*a*) Longitudinal velocity intensity. (*b*) Circumferential correlation coefficients. (*c*) Longitudinal correlation coefficient. (*d*) Circumferential velocity intensity.

paper and finally by buffing with tissue paper. Three sizes of nickel wire were used, 14, 22 and 26 B and S gauges. The rectangular electrodes had lengths L which varied from 0·003 to 0·021 in. and widths W which varied from 0·020 to 0·062 in.

As has been shown by Reiss & Hanratty (1963), the circular electrodes are sensitive to velocity fluctuations in the direction of mean flow. By making the width ten times larger than the length, the rectangular electrodes are sensitive to velocity fluctuations perpendicular to the width dimension (Mitchell 1965).

Different configurations that were used with the rectangular electrodes are shown in figure 1. Average mass-transfer rates, root-mean-square values of the fluctuations, spectral density functions and amplitude distribution functions were measured from electrodes which were oriented like the one shown in figure 1 (*a*). Circumferential correlation coefficients were measured from the configuration shown in figure 1 (*b*), for which the minimum centre-to-centre distances

between the electrodes were 0·009 in., the electrode widths were 0·003 in., and the lengths were 0·03 in. Longitudinal correlation coefficients were determined from the configuration shown in figure 1(*c*). The smallest spacing between the electrodes in this group was 0·05 in. The electrodes were very carefully aligned perpendicular to a line along the axis of the pipe. Fluctuating velocity components in the transverse direction were measured by the method described by Hinze (1959) from electrodes oriented like those in figure 1(*d*).

4. Correction for non-uniform flow

It is desirable to make the electrodes small compared with the scale of the disturbances so that local values of the fluctuating flow can be measured. Since this turns out to be quite difficult to acomplish in the system being studied, a correction for non-uniform flow is needed. Measurements of correlation coefficients in the longitudinal and circumferential directions have indicated that the flow over the electrodes used for this study was uniform in the flow direction and non-uniform in the circumferential direction. Thus, for the rectangular electrodes the intensity of the fluctuations in the local mass-transfer coefficient $\overline{k^2}$ can be related to the measured average intensity over the electrode surface $\overline{\langle k \rangle^2}$ by

$$\overline{\langle k \rangle^2} = \frac{2\overline{k^2}}{W^2} \int_0^W (W-g)\, R(g)\, dg, \tag{3}$$

where R is the circumferential correlation coefficient. For circular electrodes

$$\overline{\langle k \rangle^2} = \frac{4\overline{k^2}}{\pi^2 a^2} \int_{-a}^{+a} \int_{-a}^{+a} [(a^2 - z_i^2)\,(a^2 - z_j^2)]^{\frac{1}{2}}\, R(g)\, dz_i\, dz_j, \tag{4}$$

where a is the radius of the circle, z is the distance from the centre of the circle to a longitudinal strip of width dz, and $g = z_i - z_j$. Equations (3) and (4), along with measured values of the circumferential correlation, were used to correct the measured intensity for non-uniform flow.

5. Relation of mass transfer measurements to the velocity field

The measured mass-transfer rates can be related to the velocity field after certain simplifying assumptions, which are justified because of the thinness of the concentration boundary layer, have been made. For sufficiently large values of W/L the velocity component along the electrode width does not affect the mass transfer. Define x as a co-ordinate axis perpendicular to W, and y as the co-ordinate axis perpendicular to the electrode surface. Let U and V be the velocities in the x- and y-directions. The flow will be assumed uniform over the electrode surface, with the consequence that U and V are functions of t and y but not of x or z. For very thin concentration boundary layers the curvature of the wall can be neglected and the mass balance for the ferricyanide ion is

$$\frac{\partial C}{\partial t} + U\frac{\partial C}{\partial x} + V\frac{\partial C}{\partial y} = D\frac{\partial^2 C}{\partial y^2}. \tag{5}$$

The boundary conditions will be taken as

$$C = C(x, y, t), \quad C(x, 0, t) = 0 \quad (0 \leqslant x \leqslant L), \tag{6a, b}$$

$$C(x, \infty, t) = C(0, y, t) = C_b. \tag{6c}$$

The axial diffusion has been neglected in (5) and (6) because the diffusion coefficient of the ferricyanide ions in the electrolyte is very small. Ling (1962) has studied the effects of the axial diffusion terms and has concluded that they may be neglected when

$$\bar{S}L^2/D > 5000, \tag{7}$$

where S is the velocity gradient. The electrodes used in this study satisfied this criterion for all Reynolds numbers at which data were taken.

Equations (5) and (6) would be applicable for the circular electrode with x being the direction of mean flow (Reiss & Hanratty 1963).

The velocities and the concentration are expressed as the sum of steady and fluctuating components,

$$U = \bar{U} + u, \quad V = \bar{V} + v, \quad C = \bar{C} + c. \tag{8}$$

For fully developed flow $\bar{V}$ is zero. Since the region affecting the mass transfer is $y^+ < 0{\cdot}5$ and since for $y^+ < 5$ the average velocity is a linear function of y, $\bar{U}$ is given by

$$\bar{U} = \bar{S}y, \tag{9}$$

where the velocity gradient $\bar{S}$ can be related to the friction velocity and the kinematic viscosity by

$$\bar{S} = u^{*2}/\nu. \tag{10}$$

In the immediate vicinity of the wall the fluctuating velocity field can be represented by

$$u = s(t, x)y, \quad v = -(\partial s/\partial x)y^2, \tag{11), (12}$$

where s is the fluctuation in the velocity gradient at the wall. It will be assumed that the concentration boundary layer is so thin that (11) is a good approximation to the velocity field and that v may be neglected.

Making use of the above assumptions the following equations describe the average and fluctuating concentration fields if second-order terms in the fluctuating quantities are neglected:

$$\bar{S}y\,\partial\bar{C}/\partial x = D\,\partial^2\bar{C}/\partial y^2, \tag{13}$$

$$\bar{C}(0, y) = \bar{C}(x, \infty) = C_b, \qquad \bar{C}(x, 0) = 0 \quad (0 \leqslant x \leqslant L), \tag{14a, b}$$

$$\frac{\partial c}{\partial t} + \bar{S}y\frac{\partial c}{\partial x} + sy\frac{\partial \bar{C}}{\partial x} = D\frac{\partial^2 c}{\partial y^2}, \tag{15}$$

$$c(x, \infty, t) = c(0, y, t) = 0, \quad c(x, 0, t) = 0 \quad (0 \leqslant x \leqslant L). \tag{16a, b}$$

The solution of (13) and (14) is

$$\frac{\bar{C}(x, y)}{C_b} = \frac{1}{\Gamma(\frac{4}{3})}\int_0^{\eta} e^{-\eta^3}\,d\eta, \tag{17}$$

where

$$\eta = y(\bar{S}/9Dx)^{\frac{1}{3}}. \tag{18}$$

Values of the integral in (17) are tabulated by Abramowitz (1951). The average mass transfer over the electrode surface is given as

$$\overline{\langle K \rangle} = \frac{1{\cdot}5}{9^{\frac{1}{3}}\Gamma(\frac{4}{3})}\left(\frac{D^2\bar{S}}{L}\right)^{\frac{1}{3}}. \tag{19}$$

Equation (19) shows how the average velocity gradient at the wall may be calculated from average mass-transfer measurements.

The solution of (15) and (16) for the general time-dependent case can be obtained by treating the concentration boundary layer like a linear element which responds to fluctuations introduced by the shear stress through (15). The shear stress and the concentrations are assumed to exhibit harmonic oscillations about their means. Thus, if

$$s = \hat{s}\exp(i2\pi nt), \quad c = \hat{c}\exp(i2\pi nt), \tag{20), (21}$$

where $\hat{s}$ is taken as real and $\hat{c}$ may be real or complex, are introduced into (15) the following is obtained

$$i2\pi n\hat{c} + \bar{S}y\frac{\partial\hat{c}}{\partial x} + \hat{s}y\frac{\partial\bar{C}}{\partial x} = D\frac{\partial^2\hat{c}}{\partial y^2}. \tag{22}$$

It is desired to evaluate from (22) the mass-transfer amplitude given as

$$\langle\hat{k}\rangle = \frac{1}{L}\int_0^L D\left(\frac{\partial\hat{c}}{\partial y}\right)_w dx. \tag{23}$$

It has been observed that fluctuations of interest are of low frequency. Therefore, it is convenient to express the real and imaginary parts of $\hat{c}$ in the following power series:

$$\hat{c}_R = \hat{c}_{R_0} + 2\pi n\hat{c}_{R_1} + (2\pi n)^2\hat{c}_{R_2} + \ldots, \tag{24}$$

$$\hat{c}_I = \hat{c}_{I_0} + 2\pi n\hat{c}_{I_1} + (2\pi n)^2\hat{c}_{I_2} + \ldots. \tag{25}$$

By substituting (24) and (25) into (22) the following equation for $\hat{c}_{R_0}$ is obtained:

$$\bar{S}y\frac{\partial\hat{c}_{R_0}}{\partial x} + \hat{s}y\frac{\partial\bar{C}}{\partial x} = D\frac{\partial^2\hat{c}_{R_0}}{\partial y^2}. \tag{26}$$

Similarly the differential equation for $\hat{c}_{I_0}$ is

$$\bar{S}y\frac{\partial\hat{c}_{I_0}}{\partial x} = D\frac{\partial^2\hat{c}_{I_0}}{\partial y^2}. \tag{27}$$

Since $\hat{c}_{I_0}$ is zero at the wall and at $y = \infty$, the only solution which is permitted is $\hat{c}_{I_0} = 0$. The solution of (26) is called the quasi-steady solution valid in the limit as $n \to 0$. It is given by the expressions

$$\hat{c}_{R_0} = \hat{s}(\partial\bar{C}/\partial\bar{S}), \quad \text{or} \quad \hat{c}_{R_0} = \tfrac{1}{3}y\,\partial\bar{C}/\partial y. \tag{28), (29}$$

The mass-transfer amplitude corresponding to this quasi-steady solution is

$$\hat{k}_S = \tfrac{1}{3}(\hat{s}/\bar{S})\,\bar{K}. \tag{30}$$

In obtaining a solution valid at higher frequencies it is first noted that the odd terms in (24) and the even terms in (25) will equal zero

$$\hat{c}_R = \hat{c}_{R_0} + (2\pi n)^2\hat{c}_{R_2} + (2\pi n)^4\hat{c}_{R_4} + \ldots, \tag{31}$$

$$\hat{c}_I = (2\pi n)\hat{c}_{I_1} + (2\pi n)^3\hat{c}_{I_3} + \ldots. \tag{32}$$

Reiss & Hanratty (1963) truncated the above series as follows:

$$\hat{c} = \hat{c}_{R_0} + i2\pi n\hat{c}_{I_1},$$

to obtain

$$A^2 = |\hat{k}|^2/\hat{k}_s^2 = 1 + (2\pi n)^2(\hat{k}_{I_1}^2/\hat{k}_s^2). \tag{33}$$

However, the addition of another term yields

$$A^2 = 1 + (2\pi n^2)\left[2\frac{\hat{k}_{R_2}}{\hat{k}_s} + \frac{\hat{k}_{I_1}^2}{\hat{k}_s^2}\right] + (2\pi n)^4\frac{\hat{k}_{R_2}^2}{\hat{k}_s^2}. \tag{34}$$

The truncation used by Reiss & Hanratty did not completely specify the n^2 term and this resulted in an over estimation of the capacitance effect of the concentration boundary layer. From dimensional reasoning it can be shown that

$$A^2 = 1 + f[(2\pi nL^{\frac{2}{3}})/(D^{\frac{1}{3}}\bar{S}^{\frac{2}{3}})]. \tag{35}$$

A solution of (22) has been obtained by direct numerical integration. The following expression, valid for small values of $[(2\pi nL^{\frac{2}{3}})/(D^{\frac{1}{3}}\bar{S}^{\frac{2}{3}})]$, was obtained from this calculation:

$$A^2 = \frac{1}{1 + 0{\cdot}060[(2\pi nL^{\frac{2}{3}})/(D^{\frac{1}{3}}\bar{S}^{\frac{2}{3}})]^2}. \tag{36}$$

The velocity intensity is calculated from the mass-transfer intensity and the spectral distribution function of the mass-transfer fluctuations W_k by

$$\frac{(\overline{s^2})^{\frac{1}{2}}}{\bar{S}} = 3\frac{(\overline{k^2})^{\frac{1}{2}}}{\bar{K}}\left[\int_0^\infty \frac{W_k(n)\,dn}{A^2}\right]. \tag{37}$$

Equations (19), (36) and (37) relating the velocity field to mass-transfer measurements depend on the neglect of second-order terms in the fluctuating quantities. The error which arises from this assumption can be checked by a method similar to the one outlined by Hinze (1959) for the hot-wire anemometer. For this purpose the mass-transfer rate is approximated by the quasi-steady value given by

$$K = \sigma S^{\frac{1}{3}}, \tag{38}$$

where $S = \bar{S} + s$. Upon expanding $S^{\frac{1}{3}}$ by the binomial series

$$K = \sigma\bar{S}^{\frac{1}{3}}\left[1 - \frac{1}{3}\frac{s}{\bar{S}} - \frac{1}{9}\frac{s^2}{\bar{S}^2} - \ldots\right]. \tag{39}$$

By subtracting the time average of (39) from (39), taking the mean square and assuming the s fluctuations are Gaussian, there results

$$\frac{\overline{k^2}}{\bar{K}^2} \simeq \frac{1}{9}\frac{\overline{s^2}}{\bar{S}^2}\left[1 - \frac{2}{9}\frac{\overline{s^2}}{\bar{S}^2}\right]. \tag{40}$$

Equation (40) indicates that for velocity intensities less than 0·5 the error in using a linear model is less than 3 %.

6. Description of the experiments

Detailed descriptions of the experiments and of the techniques are presented in theses by Reiss (1962) and by Mitchell (1965) and in publications by Reiss & Hanratty (1962, 1963). Therefore, only some of the recent developments which

are not described in the papers by Reiss & Hanratty will be outlined here. These include techniques for fabricating the rectangular electrodes and improvements in the electrical equipment used to analyse the signals.

The rectangular electrodes were made by sandwiching a piece of soft nickel sheet between two brass plates and sawing slots into the assembly with a slitting saw in a horizontal milling machine. The sandwich of the brass plates was used to hold the nickel in place during sawing and to protect the edges of the electrodes from being crimped by the saw. Each slot formed the boundary of an electrode. The quality of the electrodes made by this technique depended upon the ability of the brass plates to keep the nickel from moving during the sawing. Consequently, one side of each plate was surfaced with a fly-cutter milling tool on a vertical milling machine. This operation was done very carefully, even to the point of removing stresses from the brass plates by holding them to the mill table with double-sided tape instead of a mechanical device.

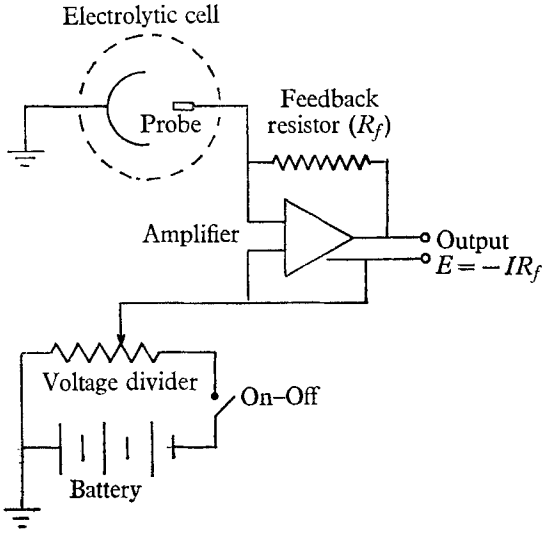

FIGURE 2. Circuit diagram of the electrical system.

The nickel was held between the machined surfaces of the brass plates and the three layers were fastened to the table of a horizontal milling machine. A bracket with the middle portion open so that the saw could contact the material held the assembly in place. The $\frac{1}{32}$ in. thick slitting saw first contacted the upper surface of the outer plate. A slot was started which was about 2 in. long but which did not extend to either end of the brass. Several progressively deeper cuts were made until the slot extended down through the upper brass plate and the nickel sheet. The saw was then extracted from the material and the mill table was moved so that another slot parallel to the first could be cut. The distance between adjacent slots determined the width of the electrode. The thickness of the nickel sheet determined its length.

Electrodes for the circumferential correlation measurements had to be built into a plastic supporting grid in order to obtain the necessary structural rigidity.

The separation distance was determined by the plastic structure, which presented excellent electrical insulation.

The electrical equipment used for earlier studies obtained the current fluctuations by measuring the voltage drop over a resistor in series with the cell. The resistor caused small voltage fluctuations to be present on the cathode of the cell. The electrical system shown in figure 2 is at present being used in order to keep the cathode voltage constant. The active element in the circuit is a Honeywell Accudata III wide band amplifier operated in the open loop mode. A six-volt storage battery supplies a constant d.c. voltage which is attenuated across a 100 Ω potentiometer. The potentiometer slide-wire is connected to the positive input and to the chassis ground of the amplifier. The cell cathode is connected to the negative input and a feedback resistor (100 kΩ to 1 MΩ) is connected between the negative input and the output of the amplifier. The current which flows through the electrode is measured as an IR drop across the feedback resistor at the output terminal. The amplifier displays a very low impedance across its input terminals resulting in voltage fluctuations on the probe of a very low level. Average IR drops from 3·0 to 8·0 V were obtained from this system without additional amplification.

The R.M.S voltage measurements, the spectral density measurements, and the correlation-coefficient determinations were performed on a Boonshaft and Fuchs Inc. Model 711 CL analyser. The amplitude distribution function was measured using a Beckman Model 7360 Universal Eput Counter and Timer.

7. Results

The use of average mass-transfer measurements to obtain $\bar{S}$ can be checked by comparing measured values of $\bar{K}$ with those calculated from (19). By a momentum balance for fully developed flow the velocity gradient at the wall can be calculated as

$$\bar{S} = U_B^2 f/2\nu \tag{41}$$

where U_B is the bulk averaged velocity. Friction factors calculated from pressure-drop measurements agreed with the Blasius equation,

$$f = 0{\cdot}079\, Re^{-\frac{1}{4}}. \tag{42}$$

Reiss & Hanratty (1963) found good agreement with circular electrodes over a variation of $\bar{S}$ of about four orders of magnitude. A test of (19) for rectangular electrodes is shown in figure 3. At Reynolds numbers less than 20,000 the data are higher than predicted. The disagreement appears to result from the smaller lengths used for the rectangular electrodes. All of the circular electrodes had L/d ratios that were greater than 0·015. This effect of length might be explained by molecular diffusion in the longitudinal direction, which was neglected in deriving (19).

Longitudinal correlation coefficients, $R_x = \overline{k_1 k_2}/\overline{k^2}$, that have been measured with the electrode arrangement shown in figure 1 (*c*) are plotted in figure 4. The distance between the electrodes x has been normalized by the longitudinal integral scale Λ_x. As indicated in figure 4 the integral scale was of the order of 0·33 to 0·54 pipe diameters. Slightly larger longitudinal scales were reported by Reiss &

Hanratty using circular electrodes. However, it is believed the results shown in figure 4 are more reliable, since measurements could be made at smaller separations and since improved methods for measuring correlation coefficients are presently being used.

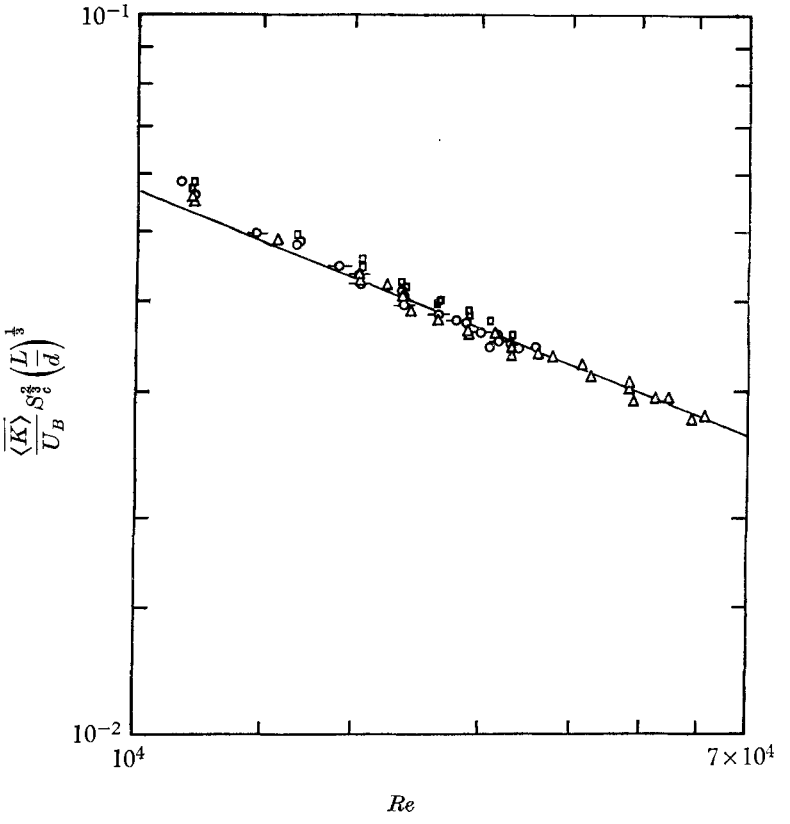

FIGURE 3. Average mass-transfer measurements. ○, $L/d = 0{\cdot}007$; □, $L/d = 0{\cdot}005$; △, $L/d = 0{\cdot}003$; –○–, $L/d = 0{\cdot}021$.

Measurements of the circumferential correlation coefficient obtained from the electrode arrangement in figure 1 (*b*) are shown in figure 5. It is to be noted that the circumferential integral scale, Λ_z, is only about one-thirtieth of the longitudinal scale. If the circumferential scale is normalized with respect to wall parameters, $\Lambda_z^+ = \Lambda_z u^*/\nu$, it does not show as much variation with Reynolds number as when it is normalized with respect to the pipe diameter. In fact,

$$\Lambda_z^+ \cong 11. \tag{43}$$

The circumferential integral scale is of the same magnitude as the region in which the average velocity profile is affected by molecular viscosity.

The effect of non-uniform flow across an electrode is shown in figure 6, where the mass-transfer intensity is plotted for a fixed length of electrode for two different widths. It is seen that the intensity of the signal decreases as the width increases. This shows the averaging effect over the electrode surface. These

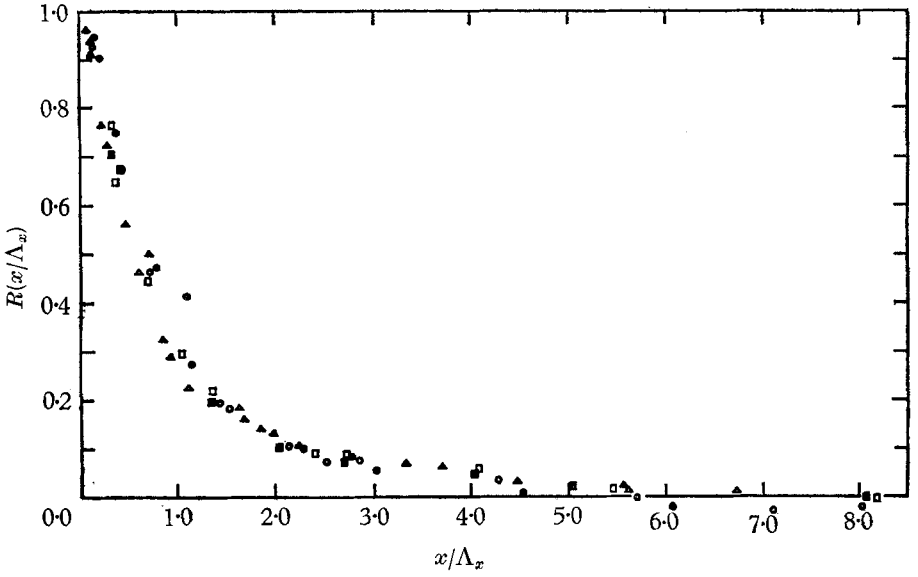

FIGURE 4. Longitudinal correlation coefficients.

	Re	Λ_x/d		*Re*	Λ_x/d
○	17,900	0·330	■	30,800	0·367
●	17,000	0·351	△	50,300	0·445
□	41,000	0·372	▲	60,700	0·540

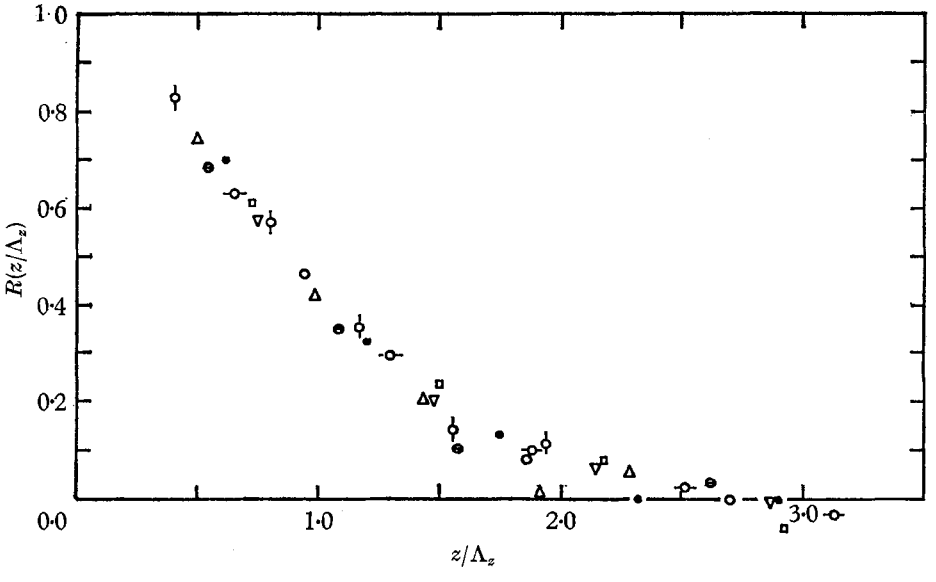

FIGURE 5. Circumferential correlation coefficients.

	Re	Λ_z/d		*Re*	Λ_z/d
○	7,500	0·022	□	14,500	0·013
△	10,200	0·018	—○—	14,900	0·014
●	11,500	0·015	▽	16,500	0·012
⊖	12,000	0·017	○	23,800	0·010

measurements have been corrected for non-uniform flow by (3) using the correlation measurements shown in figure 4. The open points in figure 6 indicate the corrected measurements. Good agreement is obtained between the two widths. It is to be noted that the effect of non-uniform flow is significant even for electrodes with widths as small as 0·03 in.

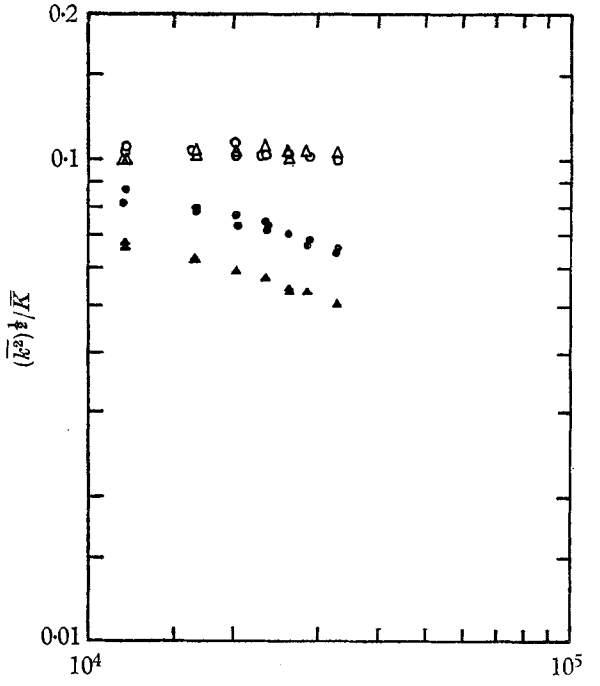

FIGURE 6. Mass-transfer intensities from electrodes with different widths.

		W/d	L/d
Corrected	○	0·033	0·003
	△	0·062	0·003
Not corrected	●	0·033	0·003
	▲	0·062	0·003

The spectral density function of the mass-transfer fluctuations, defined as

$$\overline{k^2} = \int_0^\infty W_k(n)\,dn, \tag{44}$$

is plotted in figure 7. As has been pointed out by Reiss & Hanratty, normalization with bulk parameters U_B and d does a better job of bringing together the data at different Reynolds numbers than does normalization with the wall parameters u^* and ν. It is found that the frequencies of the fluctuations are low:

$$\text{median frequency} = 0{\cdot}18 U_B/d. \tag{45}$$

Mass-transfer intensities measured from electrodes with different lengths that have been corrected for non-uniform flow are shown in figure 8. It is seen that for

the range displayed the electrode length is not affecting the intensity. Slightly larger lengths were used with the circular electrodes and, as would be expected from (37), the intensity decreases with the increase in length.

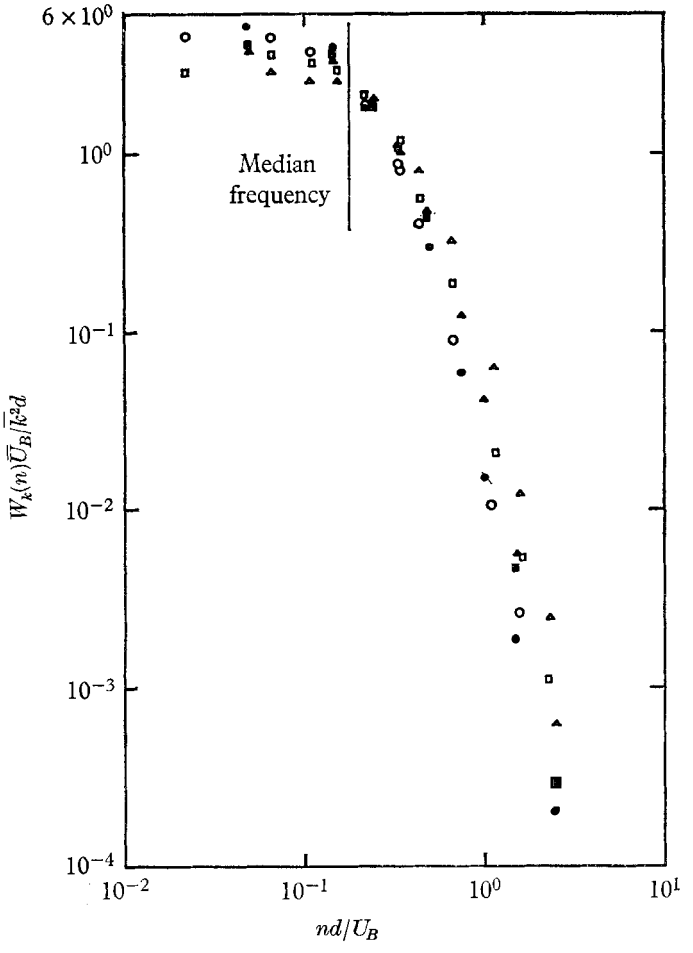

FIGURE 7. Mass-transfer spectra functions.

	L/d	Re		L/d	Re
○	0·007	22,900	■	0·005	10,500
●	0·007	10,500	△	0·003	22,900
□	0·005	22,900	▲	0·003	10,500

Velocity intensities calculated from (37), (3) and (4) are plotted in figure 9 for rectangular electrodes of three different lengths and for the circular electrodes with diameters of 0·0156 in. and 0·0252 in. The response function departs from the quasi-steady function by less than 6 % for the three rectangular electrodes and by approximately 20 % for the circular electrodes. The agreement among the different electrodes is within 3 %. This gives support to the methods used to calculate the fluctuating velocity field from the mass-transfer measurements. It

is found that the velocity fluctuations are large compared with the local average velocity in the immediate vicinity of the wall

$$[(\overline{u^2})^{\frac{1}{2}}/\overline{U}]_w = (\overline{s^2})^{\frac{1}{2}}/\overline{S} = 0{\cdot}32. \tag{46}$$

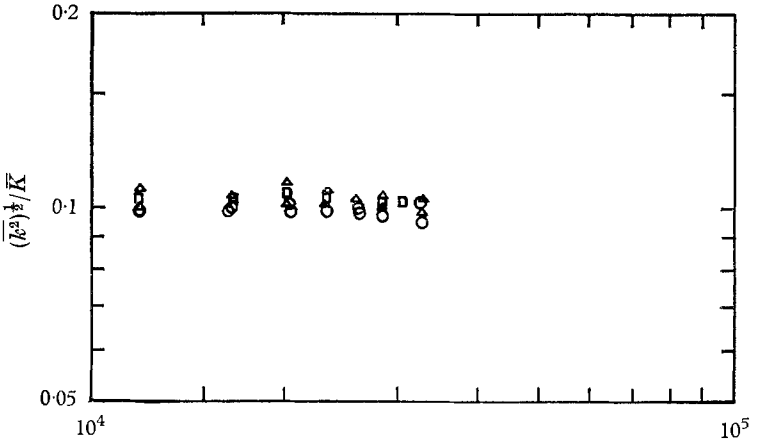

FIGURE 8. Mass-transfer intensity at different lengths.

	L/d	*W/d*
○	0·007	0·030
□	0·005	0·030
△	0·003	0·033

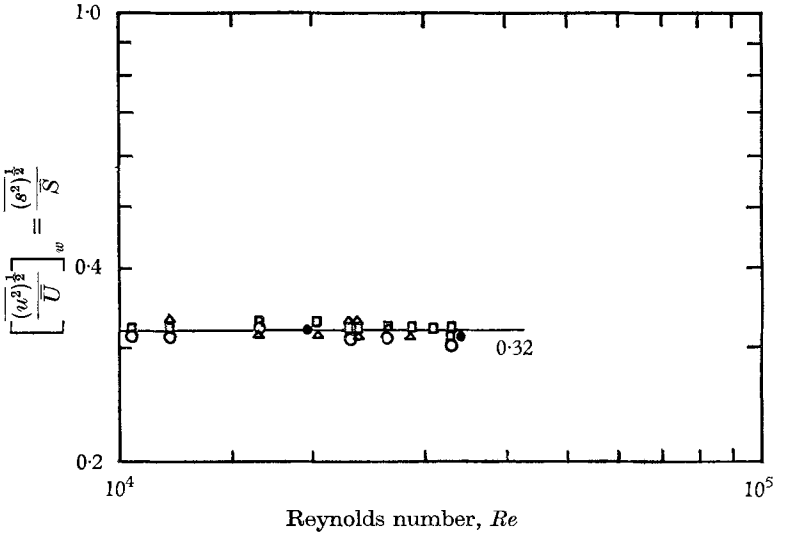

FIGURE 9. Velocity intensity at the wall.

	L/d	*W/d*
○	0·007	0·030
□	0·005	0·030
△	0·003	0·033
●	Reiss data recalculated	

This limiting intensity appears to be independent of Reynolds number. It is considerably larger than the lower limit reported by Reiss & Hanratty. This improvement in the estimate arises from the accurate treatment of the effects of non-uniform flow and of the time response of the concentration boundary layer.

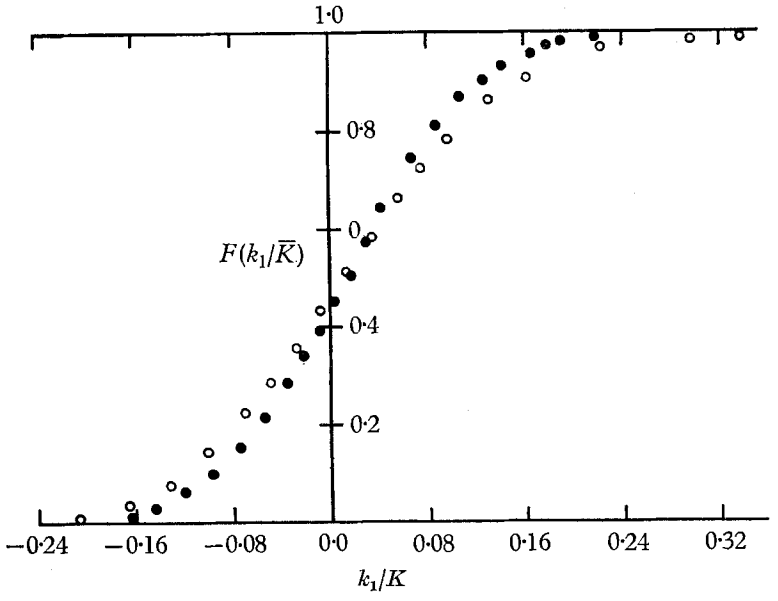

FIGURE 10. Amplitude distribution function of mass-transfer rate. ○, Re = 10,500; ●, Re = 25,000.

Two amplitude distribution functions defined as

$$F(k_1/\bar{K}) = [\text{time}\,(k/\bar{K} < k_1/\bar{K})]/\text{total time} \tag{47}$$

are shown in figure 10 for an electrode whose L/d and W/d ratios were 0·007 and 0·035 respectively. Amplitude density functions of the velocity were calculated from these data by graphical differentiation and by application of the correction for non-uniform flow and the quasi-steady response function for the boundary layer. The quasi-steady response function was used because the departure of the response factor calculated for this electrode was less than 6 %. The density function shown in figure 11 is slightly skewed toward the high-velocity side. The most interesting aspect of the results in figure 11 is that there are both positive and negative deviations from the mean of the same magnitude as the mean. It is not possible to tell whether there are occasional instantaneous velocities near the wall which are negative but the possibility is indicated by the data.

An attempt has been made to calculate the frequency spectra for the velocity fluctuations from that for the mass-transfer fluctuations. Measurements of the circumferential length scale appear approximately independent of frequency over the range shown in figure 12. This study was limited to frequencies as high as 30 c/s because for higher frequencies the signal-to-noise ratio on the tape recorder was too small. The frequency spectra for the velocity fluctuations have been calculated from the results in figure 8 using (36) and (3), with the correlation

coefficient assumed to be independent of frequency. Figure 13 presents the results. The results at high frequencies must be regarded as tentative owing to the uncertainty of the accuracy of (36) and of the constancy of the circumferential scale at high frequencies.

In order to estimate the velocity fluctuations in the circumferential direction measurements were made with the electrode configuration shown in figure 1 (*d*)

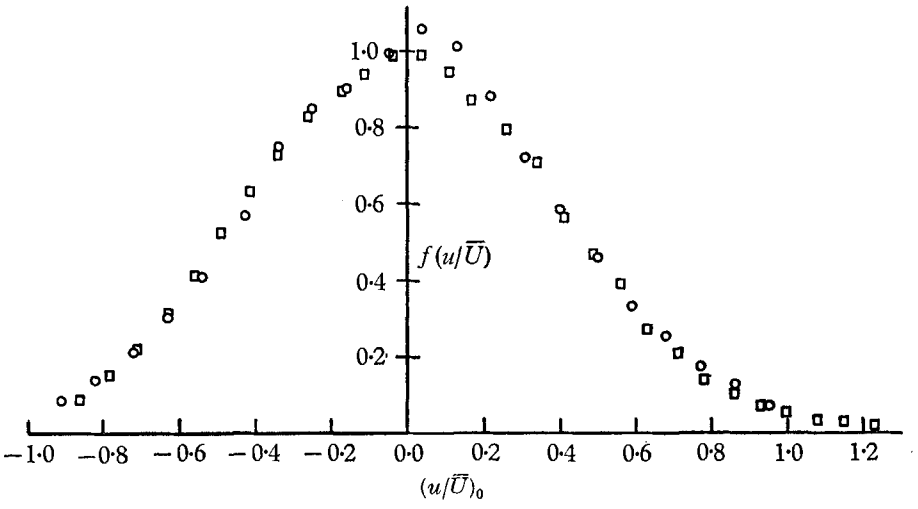

FIGURE 11. Amplitude density function of the relative intensity.
○, Re = 25,000; □, Re = 10,500.

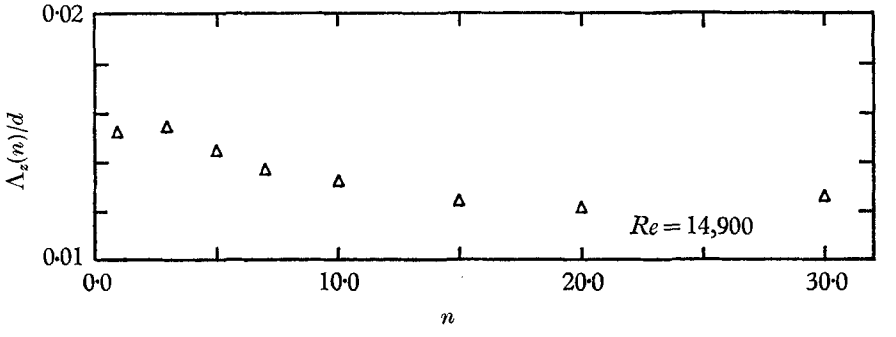

FIGURE 12. Frequency dependence of circumferential scale.

using electrodes with L/d and W/d ratios of 0·005 and 0·050 respectively. The results are shown in table 1. The estimation of the velocity fluctuation in the circumferential direction does not seem warranted since it is not certain that the differences for the measurements at different angles is significant. Nevertheless, unless the scale of the w-fluctuation is much smaller than that for the u-fluctuation it would seem that the w-velocity component is much smaller than the u-velocity component in the immediate vicinity of the wall.

Finally, it should be pointed out that the results indicate two kinds of parametric dependence. The velocity intensity, amplitude density function, and

circumferential integral scale are all independent of the Reynolds number when correlated by wall parameters u^* and ν. (Note that $\bar{S} = u^{*2}/\nu$.) On the other hand, the spectral density function and the longitudinal integral scale appear to depend upon bulk parameters such as the average velocity and the pipe diameter.

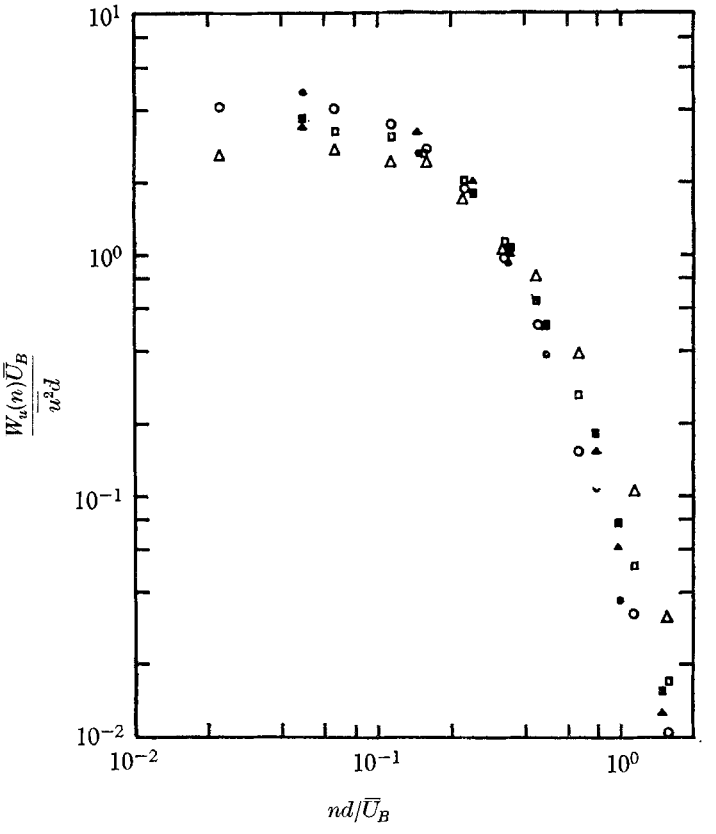

FIGURE 13. Velocity spectra.

	L/d	Re		L/d	Re
○	0·007	22,900	■	0·005	10,500
●	0·007	10,500	△	0·003	22,900
□	0·005	22,900	▲	0·003	10,500

Reynolds number	angle	intensity $(\overline{k^2})^{\frac{1}{2}}/\bar{K}$
10,000	90°	0·100 ± 0·006
10,000	45°	0·105 ± 0·006
10,000	135°	0·104 ± 0·006
25,000	90°	0·103 ± 0·006
25,000	45°	0·107 ± 0·006
25,000	135°	0·107 ± 0·006

TABLE 1

8. Comparison of results with other measurements

A comparison will now be made of the results of this research with other studies of turbulence close to a wall.

Fluctuating velocities have been measured with the hot-wire anemometer by Laufer (1954) and Sandborn (1955) in pipes, by Laufer (1951) in a two-dimensional channel, and by Klebanoff (1954) and Grant (1958) in a boundary layer over a flat plate. The velocity fluctuations in the longitudinal direction have been

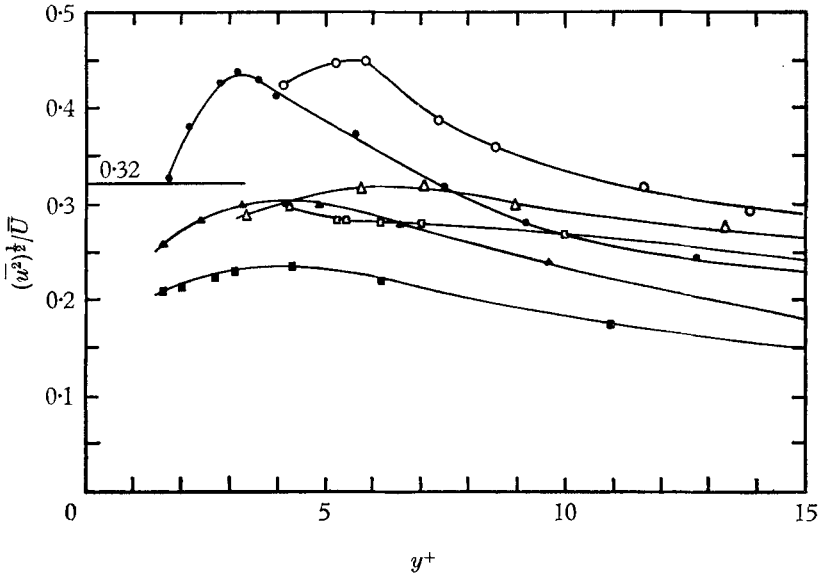

FIGURE 14. Local turbulent velocity intensities.

	Reference	Re_a		Reference	Re_a
○	Klebanoff	80,000	●	Laufer 1951	9,820
□	Laufer 1954	20,300	▲	Laufer 1951	25,000
△	Laufer 1954	215,000	■	Laufer 1951	50,000

normalized with respect to the local average velocity and plotted against y^+ in figure 14. It is quite difficult from these measurements to establish the limiting value of the intensity as $y^+ \to 0$. Nevertheless, it does appear that the value of $[(\overline{u^2})^{\frac{1}{2}}/\overline{U}]_w = 0{\cdot}32$ obtained from this study is bracketed by the intercepts suggested by the hot-wire anemometer measurements. It is quite possible that the differences among the different sets of data shown in figure 14 are not real and merely indicate the accuracy of these measurements. All of these measurements are plotted using law-of-the-wall parameters in figure 15. The solid line represents the relationship between $(\overline{u^2})^{\frac{1}{2}}/u^*$ and y^+ in the neighbourhood of $y^+ = 0$ calculated from (46). It appears that this limiting relation describes the data to distances from the wall as far as $y^+ = 7$.

The measurements of $\overline{w^2}$ by Laufer (1954) indicate that $\overline{w^2}$ is much smaller than $\overline{u^2}$ close to a wall. The results of table 1 seem to confirm this result.

One of the interesting results of the research reported in this paper and in the paper by Reiss & Hanratty (1963) is the extremely small circumferential scale. Whereas the longitudinal scale appears to be of the same magnitude as those reported for the central regions of the pipe, the circumferential scale is at least one order of magnitude smaller at the wall than at the central regions (Hinze 1959).

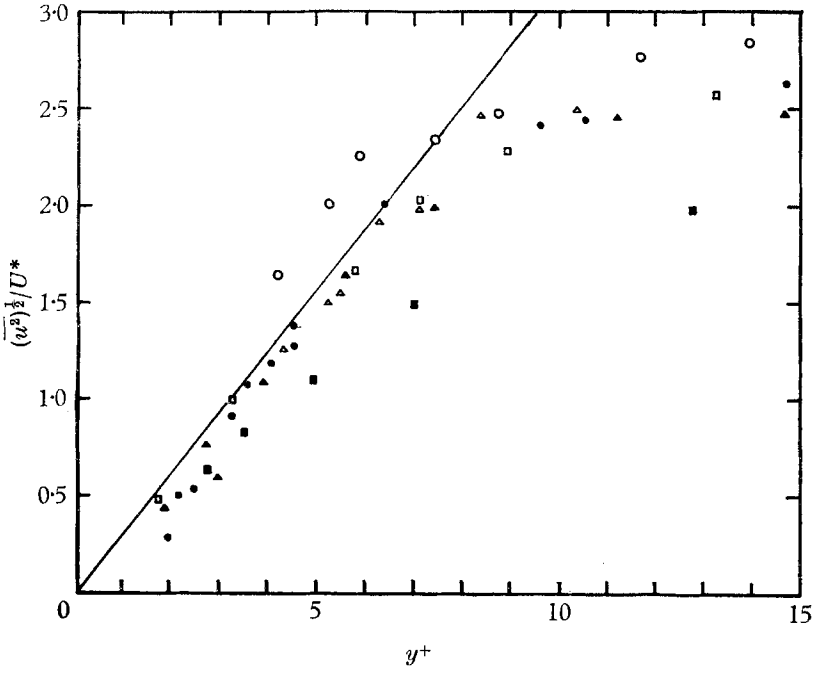

FIGURE 15. Dimensionless fluctuating velocity profile.

	Reference	Re_a		Reference	Re_a
○	Klebanoff	80,000	●	Laufer 1951	9,820
□	Laufer 1954	20,300	▲	Laufer 1951	25,000
△	Laufer 1954	215,000	■	Laufer 1951	50,100

The frequency spectra of the velocity fluctuations in the direction of flow at several values of y^+ and of the pressure fluctuations on a transducer embedded at the wall (Harrison 1958) are compared with velocity spectra obtained from rectangular and circular electrodes in figure 16. The characteristic lengths and velocities that were used are as follows: for a pipe, the radius and the bulk-averaged velocity; for a channel, the half width and the bulk-averaged velocity; for a boundary layer, the thickness and the free-stream velocity. Although this choice of normalization parameters brings together the measurements with the hot-wire anemometer in the pipe, channel and boundary layer, there is considerable difference between these and the measurements with the electrodes. The velocity spectral density functions at the wall contain smaller contributions in the high-frequency range than those reported at other points within the viscous sub-layer. The reason for this change in the shape of the spectral density function

through the viscous sub-layer is not understood as yet. The shape of the spectral density function obtained from the electrodes appears to be close to that for the pressure fluctuations. However, the integral scales are quite different.

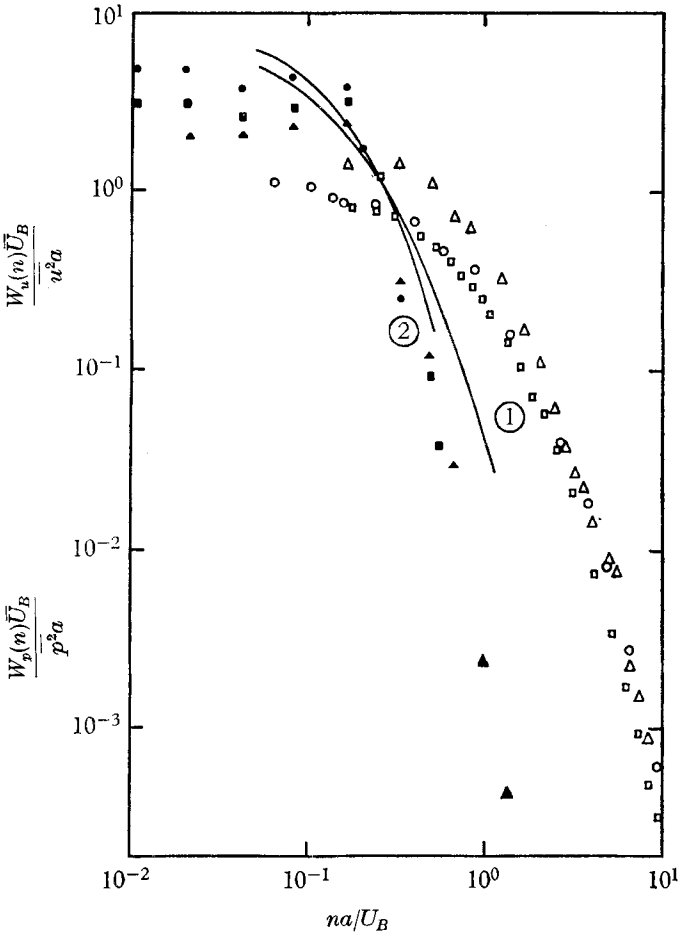

FIGURE 16. Comparison of spectra from the viscous sub-layer.

	Velocity spectra				Pressure spectra		
	Reference	Re_a	y^+		Reference	U_B (cm/sec)	y^+
△	Sanborn	20,300	2·72	▲	Harrison	1,500	Wall
□	Laufer 1951	25,000	5·90	■	Harrison	3,000	Wall
○	Klebanoff	80,000	3·13	●	Harrison	6,000	Wall
①	Reiss		< 0·5				
②	Mitchell		< 0·5				

Scales of the pressure fluctuations at a wall have been measured by Willmarth & Wooldridge (1962). These show a much larger scale in the transverse direction than do the velocity fluctuations. This would seem to indicate that the velocity field close to the wall may not be looked upon as a region which is not simply reacting to the pressure fluctuations.

Runstadler, Kline & Reynolds (1963) have studied streak patterns at the

wall resulting from dye injection into the boundary layer and have argued that the streaks near the wall are caused by regions of very low velocities. Support for this explanation is obtained from the amplitude distribution function (figure 11), which suggests the existence of velocities close to zero. Similar experiments to those performed by Runstadler, Kline & Reynolds have been carried out in the same system in which the electrode studies were performed. A dark plume of dye was formed on an electrode mounted flush to a wall by the electrochemical production of iodine in a starch solution. The same type streaks as had been noted by Runstadler, Kline & Reynolds were observed. The average distance between the streaks was estimated to be about $z^+ = 50$. There is considerable uncertainty in how to count these streaks and the above figure must be regarded as only a rough estimate. It is close to the value $z^+ = 76{\cdot}5$ reported by Runstadler, Kline & Reynolds for boundary-layer flows.

9. Linearized model of the wall region

Sternberg (1961) has suggested a linearized model of the viscous sub-layer wherein the flow fluctuations are controlled by pressure fluctuations imposed from outside the sub-layer. The velocity fluctuations in the x-direction are represented by the equation

$$\frac{\partial u}{\partial t} = -\frac{1}{\rho}\frac{\partial p}{\partial x} + \nu\frac{\partial^2 u}{\partial x^2}. \tag{48}$$

The solution presented by Sternberg can be used to relate Fourier components of the pressure and velocity fluctuations at the wall

$$\overline{s_x^2} = (c^2\overline{p^2}\omega)/(\rho^2\nu). \tag{49}$$

The results reported in this paper do not support the model proposed by Sternberg. The scale of the velocity field in the circumferential direction is much smaller than that for the pressure field. In addition, equation (49) would indicate that the magnitudes of the measured pressure fluctuations are not large enough to account for the measured $\overline{s_x^2}$.

It would appear that in a layer near the wall in which (48) is valid the velocity fluctuations are the result of shear fluctuations imposed upon the layer from the fluid outside. Likewise, it would appear that there is no region close to the wall in which $\partial u/\partial t \cong -(1/\rho)(\partial p/\partial x)$. If a linearized model is to describe some aspects of the flow close to a wall, then the complete linearized equations must be used and the hypothesis that the flow field in the viscous sub-layer is directly related to fluctuating pressure field must be disregarded.

Such an analysis has been carried out and is reported in a thesis by one of the authors (Mitchell 1965). However, although agreement is obtained between some aspects of the measurements reported in this paper and these calculations the assumptions made are questionable enough that it does not seem appropriate to present them without further work.

This research is sponsored by the Air Force Office of Scientific Research, Office of Aerospace Research, United States Air Force, under AFOSR Grant Nr AFOSR-547.

REFERENCES

ABRAMOWITZ, M. 1951 *J. Math. Phys.* **20**, 162.

EISENBERG, M., TOBIAS, C. W. & WILKE, C. R. 1954 *J. Electrochem. Soc.* **103**, 413.

GORDON, S. L. & TOBIAS, C. W. 1963 M.Sc. thesis, Univ. of California at Berkeley.

GRANT, H. L. 1958 *J. Fluid Mech.* **4**, 149.

HARRISON, M. 1958 *David Taylor Model Basin, Hydromech. Lab. Res. & Development Rept* no. 1260.

HINZE, J. O. 1959 *Turbulence.* New York: McGraw-Hill.

KLEBANOFF, P. S. 1954 *NACA TN* no. 3187.

LAUFER, J. 1951 *NACA TR* no. 1053.

LAUFER, J. 1954 *NACA TR* no. 1174.

LING, S. C. 1962 *J. Heat Trans.* C **85**, 230.

MITCHELL, J. E. 1965 Investigation of wall turbulence using a diffusion controlled electrode. Ph.D. thesis in Chemical Engineering, Univ. of Illinois, Urbana.

REISS, L. P. 1962 Investigation of turbulence near a pipe wall using a diffusion controlled electrolytic reaction on a circular electrode. Ph.D. thesis in Chemical Engineering, University of Illinois, Urbana.

REISS, L. P. & HANRATTY, T. J. 1962 *A.I.Ch.E. J.* **8**, 245.

REISS, L. P. & HANRATTY, T. J. 1963 *A.I.Ch.E. J.* **9**, 154.

RUNSTADLER, P. W., KLINE, S. J. & REYNOLDS, W. C. 1963 An experimental investigation of the flow structure of the turbulent boundary layer. *Rept MD-8, Dept. of Mech. Engng*, Stanford Univ.

SANDBORN, V. A. 1955 *NACA TN* no. 3266.

STERNBERG, J. 1961 A Theory for the Laminar Sublayer in Turbulent Flow, *Rept* no. 1127, *Ballistic Res. Lab.*, Aberdeen Proving Ground, Maryland.

WILLMARTH, W. W. & WOOLDRIDGE, C. E. 1962 *Repts* 02920-1-T and 02920-2-T *Dept of Aero. & Astro. Engng*, Univ. of Michigan, Ann Arbor.